

Temperature dependent vibrational Raman lidar effective backscatter cross-section due to narrow-band interference filter usage

Michael Haimerl^(a), Nikos Siomos^(a), Volker Freudenthaler^(a)

(a) Central facility ACTRIS LMU, Munich

Meteorologisches Institut München, Theresienstraße 37, 80333 München, Germany

Lead Author e-mail address: m.haimerl@lmu.de

Abstract: We analyze and discuss the temperature dependent anomalies introduced into the rotational-vibrational (ro-vibrational) Raman signals due to angular-truncated transmission through interference filters (IF). For that we use equations for ro-vibrational Raman scattering proposed by literature to calculate the molecular backscatter cross-sections of N₂. The results allow us to quantify the extend of these temperature dependent anomalies with respect to the interference filter characteristics such as the central wavelength and bandwidth. As a preliminary result it turned out that transmission through narrow-band interference filters introduces only small anomalies.

1. Introduction

When electromagnetic radiation interacts with molecules, elastic and inelastic scattering processes occur whereby the latter ones in most of the cases change the wavelength of the scattered light with respect to the incident one. While both processes are equally important for the various lidar measurement techniques, this abstract will focus onto the inelastic scattering processes, the so-called Raman scattering. In particular, we deal with the temperature dependence of the ro-vibrational Raman backscatter spectra due to the transmission limit through narrow-band interference filters. To analyze the consequence of the changing temperature we use the equations published by M. Adam [1] to calculate the temperature dependent ro-vibrational Raman backscatter cross section for the N₂ molecule. These models have been implemented as part of ARC by the CARS research group in ACTRIS [5]. The results allow us to quantify the extend of the temperature dependence considering the central wavelength and bandwidth of the IF. In the following we assume that readers of this abstract are familiar with the theory of Raman scattering and its application in atmospheric research with lidars. Therefore, we will leave away any details (see cited literature) and focus on the important aspects of our work.

2. Raman scattering

The theory of Raman scattering in atmospheric physics describes inelastic, non-resonant scattering of electromagnetic radiation by

molecules. In the case of Anti-stokes Raman scattering the wavelength of the photons becomes blue-shifted. The opposite happens for Stokes scattering, resulting in red-shifted scattered light. These wavelength shifts are caused by transitions between the different ro-vibrational energy levels of the molecules as part of the scattering process. These energy levels, so also the resulting scattering spectra, are characteristic for each molecule [2-4]. For our calculations we use the equations for the differential backscattering cross section of ro-vibrational Raman scattering given by [1]:

$$\left(\frac{\partial\sigma}{\partial\Omega}\right)_{T,J} = (2\pi)^4 \cdot (\nu_0 - \nu_{vib} + \Delta\nu_J)^4 \cdot F_{MB}(T,J)\Phi'_J \quad (1)$$

Hereby, T denotes the environmental temperature and J the rotational quantum number. The wavenumber of the emitted laser light is given by ν_0 , the wavenumber shift of the first vibrational Stokes spectral lines is represented by ν_{vib} and the wavenumber shift of the rotational energy levels $\Delta\nu_J$. According to [1] we consider only ro-vibrational lines of N₂ with a quantum number of $\nu = 1$.

The temperature dependence of $\left(\frac{\partial\sigma}{\partial\Omega}\right)$ is introduced by the Maxwell-Boltzmann distribution function for ro-vibrational Raman scattering according to [1].

$$F_{MB}(T,J) \sim \frac{(2J+1) \exp\left(-\frac{E_{rot,J}}{K_B T}\right)}{Q_{rot}(T) \cdot \left(1 - \exp\left(-\frac{h c \nu_{vib}}{K_B T}\right)\right)} \quad (2)$$

$Q_{rot}(T)$ stands for the partition function of the rotational Raman scattering part, $E_{rot,J}$ denotes the rotational energy levels and K_B is the Boltzmann constant. We calculate differential backscatter cross sections up to $J = 101$. Moreover, we only consider the vibrational Stokes cross-sections. The anti-Stokes cross-sections are smaller by several orders of magnitude and are therefore naturally out of interest [2].

For calculating the total backscatter cross-section of N_2 we sum over all spectral lines of interest and multiply it with the relative concentration of N_2

$$\sigma_{bsc,i} = c_{N_2} \cdot \sum_J \left(\frac{\partial \sigma}{\partial \Omega} \right)_{T,J} \quad (3)$$

For more detailed information about the presented equations please refer to [1].

3. Application of interference filters to the spectra

When an IF is applied, we simply weight each spectral line with the transmission function of the IF. The effective backscatter cross-section is provided by the following expression

$$\sigma_{bsc,i}^{eff} = \sigma_{bsc,i} \cdot IF(\nu_0 - \nu_{vib} + \Delta\nu_J) \quad (4)$$

For our study we used theoretical Lorentzian and Gaussian shaped IF as well as real available double-cavity filters (see Fig. 1) with two different bandwidths.

The effect of applying a filter to the line spectra is illustrated in Fig. 2.

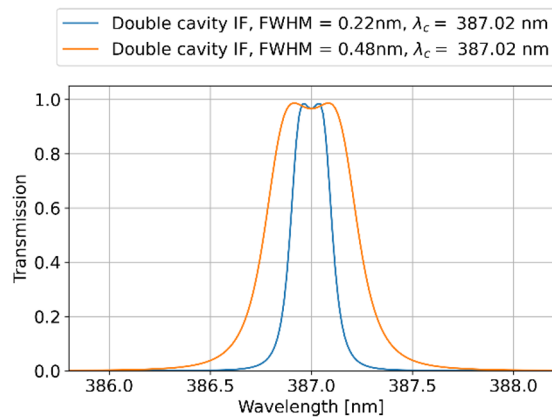


Figure 1. Available double cavity interference filters for ro-vibrational Raman spectrum of N_2 centered around 387.02 nm.

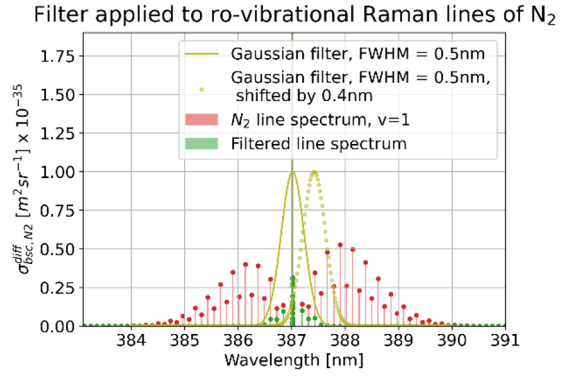


Figure 2. Application of a centered and a shifted Gaussian shaped IF.

As shown in Fig. 2 by the dotted filter graph, we also study the effect of an IF being off-center to the central vibrational line, as small wavelength shifts can occur due to temperature changes in the laser rod. Also, a change of the incidence angle of the detected light to the IF appears as a shift of the IF with respect to the central spectral line along the wavelength axis. These two aspects make the analysis of shifted IF interesting.

4. Temperature dependence of the total backscatter cross section with applied filters

As we naturally have distinct temperature variations due to the atmospheric temperature profile, we calculate the backscattered spectra for different altitudes corresponding to different temperatures according to the US standard atmosphere 1976 model.

The relative difference χ between the two most extreme temperatures, i.e. near the ground and around 15 km, is shown in Eq. 5:

$$\chi [\%] = \frac{\sigma_{bsc,N_2}^{eff}(15\text{km}) - \sigma_{bsc,N_2}^{eff}(0\text{km})}{\sigma_{bsc,N_2}^{eff}(0\text{km})} \cdot 100 \quad (5)$$

Fig. 3 shows the effective backscatter cross section for different IF shapes and bandwidths plotted along the altitude. The effective backscatter cross sections for IF with small or large bandwidths do not show a strong altitude dependence. However, for bandwidths between 1 nm and 5 nm appears an increase of the effective backscatter cross section with altitude. This increase stops when the atmospheric tropopause around 11 km is reached.

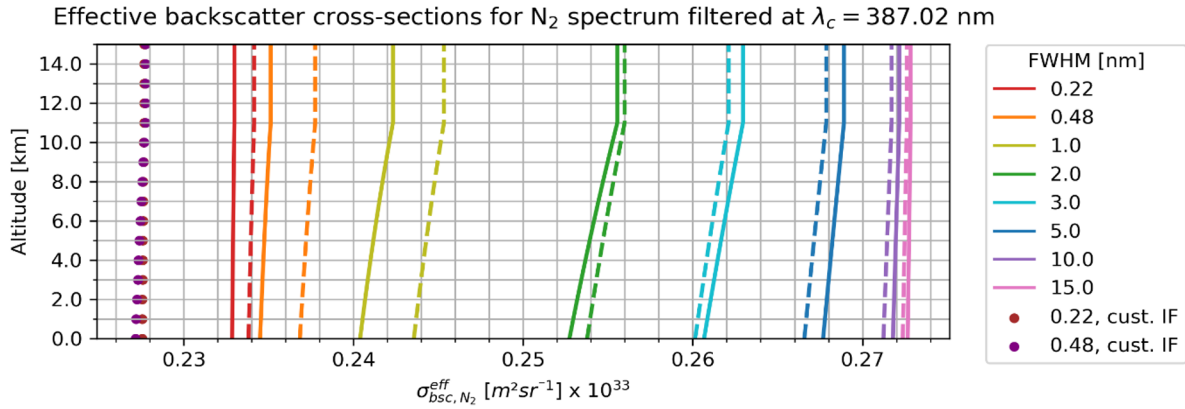


Figure 3. Effective backscatter cross-section variation for N_2 ro-vibrational spectrum along altitude from 0 to 15 km. Full lines correspond to Gaussian shaped filters or double cavity filters. Dashed lines belong to Lorentzian shaped filters.

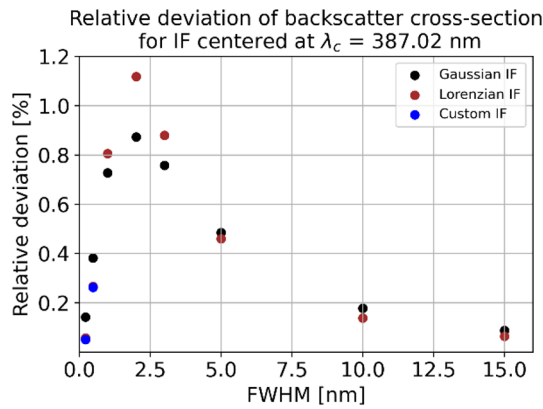


Figure 4. Relative deviation χ of the effective total backscatter cross-section due to temperature dependence according to Eq. 5 plotted over the FWHM (Full-width-half-maximum) of the according IF.

In Fig. 3 and Fig. 4 we see that the small bandwidth custom IF show only little relative Deviations χ , below 0.4%. Filters with middle size bandwidth about up to 4 nm are more affected. Here also the shape of the transmission function matters. The relative deviations χ decrease again for FWHMs of 5 nm and more. The plot in Fig. 5 shows the effect of applying IFs with the center wavelength shifted with respect to the central spectral line (see Fig. 1) of the ro-vibrational spectrum of N_2 . (see Fig. 2). As Lorentzian shaped filters and Gaussian ones with equal FWHM show a similar behavior, the Lorentzian shaped filters are omitted here.

We clearly see that the larger the shift the larger the relative deviation χ are for small bandwidth filters.

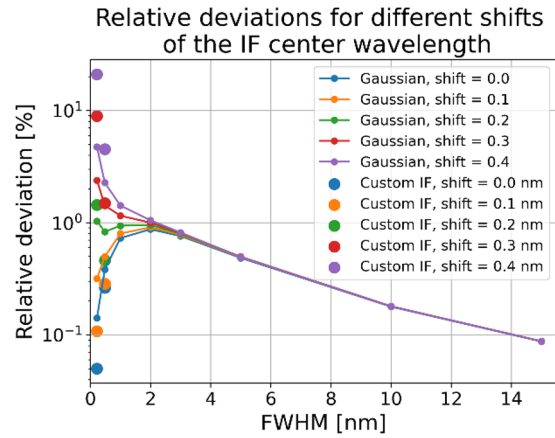


Figure 5. Relative deviations χ of effective total backscatter cross-section for two different double-cavity IFs and different Gaussian shaped IFs shifted with respect to the center wavelength of the ro-vibrational spectrum of N_2 .

The smaller the filter bandwidth the more the central spectral line (see Fig. 2) is attenuated in case of a shift. Since, this line contributes strongly to the total backscatter cross-section, the smaller filters are more sensitive to shifts away from it causing the effective cross-section to deviate up to 2 orders of magnitude. A difference in relative deviation χ over several orders magnitude therefore is a reasonable outcome. All curves reach a small plateau around 2 nm FWHM, and above 3 nm the deviations decrease further for increasing bandwidths. This is because the shift of the center wavelength of the filter becomes small compared to its FWHM. Consequently, most of the spectrum, especially the central always lies in the filter region with little change in transmission over wavelength.

5. Conclusion

For this abstract we extended the ATLAS software from pure rotational Raman scattering by vibrational Raman scattering according to the model of M. Adam [1]. Additionally, we were able to show the temperature dependence of the effective backscatter cross-section when using narrow-band IF centered around the Q-branch of the N₂ Stokes ro-vibrational spectrum. We did the same for IF shifted with respect to the Q-branch. For the future, it would be interesting to analyze also this effect for a laser wavelength of 532 nm and to consider more and different real IF.

According to the so far gathered results we generally can summarize that using filters with small bandwidths the backscatter cross section is affected least by temperature change along altitude. The same could be found for IF with large bandwidth.

However, these results still need to be treated carefully as we did not yet provide any calculations on how our results affect e.g. the extinction profile and other parameters.

6. Acknowledgements

This project receives funding from the European Union's Horizon research and innovation program under grant agreement No. 871115. ACTRIS-D is funded by the German Federal Ministry for Education and Research (BMBF) under grant agreements 01LK2001A-K & 01LK2002A-G.

7. References

- [1] M. Adam, "Notes on Temperature-Dependent Lidar Equations", *AMetSoc* Vol. 26, 1021–1039 (2009).
- [2] U. Waninger, "Raman lidar" (C. Weitcamp, „Lidar, Range-Resolved Optic Remote Sensing of the Atmosphere“, *Optical science*, 241-271 (2005).
- [3] C.-Y. She, "Spectral structure of laser light scattering revisited: bandwidths of non-resonant scattering lidars", *AO* Vol. 40, 4875-4884 (2001).
- [4] A. Berhendt, T. Nakamura, „Calculation of the calibration constant of polarization lidar and its dependency on atmospheric temperature“, *OE* Vol. 10, 805-817 (2002).
- [5] N. Siomos et al., "Rotational Raman Scattering Through Narrow-Band Interference Filters: Investigating Uncertainties Using a New Rayleigh Scattering Code Developed within ACTRIS", Sullivan, J.T., et al. *ILRC 2022. Spring Atmospheric sciences* (2022).